SUPPLEMENTARY INFORMATION
https://doi.org/10.1038/s41593-018-0093-5

nature neuroscience

In the format provided by the authors and unedited.

Cortico–reticulo–spinal circuit reorganization enables functional recovery after severe spinal cord contusion

Leonie Asboth[1,6], Lucia Friedli[1,6], Janine Beauparlant[1,6], Cristina Martinez-Gonzalez[1], Selin Anil[1], Elodie Rey[1], Laetitia Baud[1], Galyna Pidpruzhnykova[1], Mark A. Anderson[1], Polina Shkorbatova[1,2], Laura Batti[3], Stephane Pagès[3], Julie Kreider[1], Bernard L. Schneider[4], Quentin Barraud[1] and Gregoire Courtine[1,5]*

[1]Center for Neuroprosthetics and Brain Mind Institute, School of Life Sciences, Swiss Federal Institute of Technology (EPFL), Geneva, Switzerland. [2]Pavlov Institute of Physiology RAS, St. Petersburg, Russia. [3]Wyss Center for Bio and Neuroengineering, Campus Biotech, Geneva, Switzerland. [4]Brain Mind Institute, School of Life Sciences, Swiss Federal Institute of Technology (EPFL), Lausanne, Switzerland. [5]Department of Neurosurgery, University Hospital of Lausanne (CHUV), Lausanne, Switzerland. [6]These authors contributed equally: Leonie Asboth, Lucia Friedli and Janine Beauparlant.
*e-mail: gregoire.courtine@epfl.ch

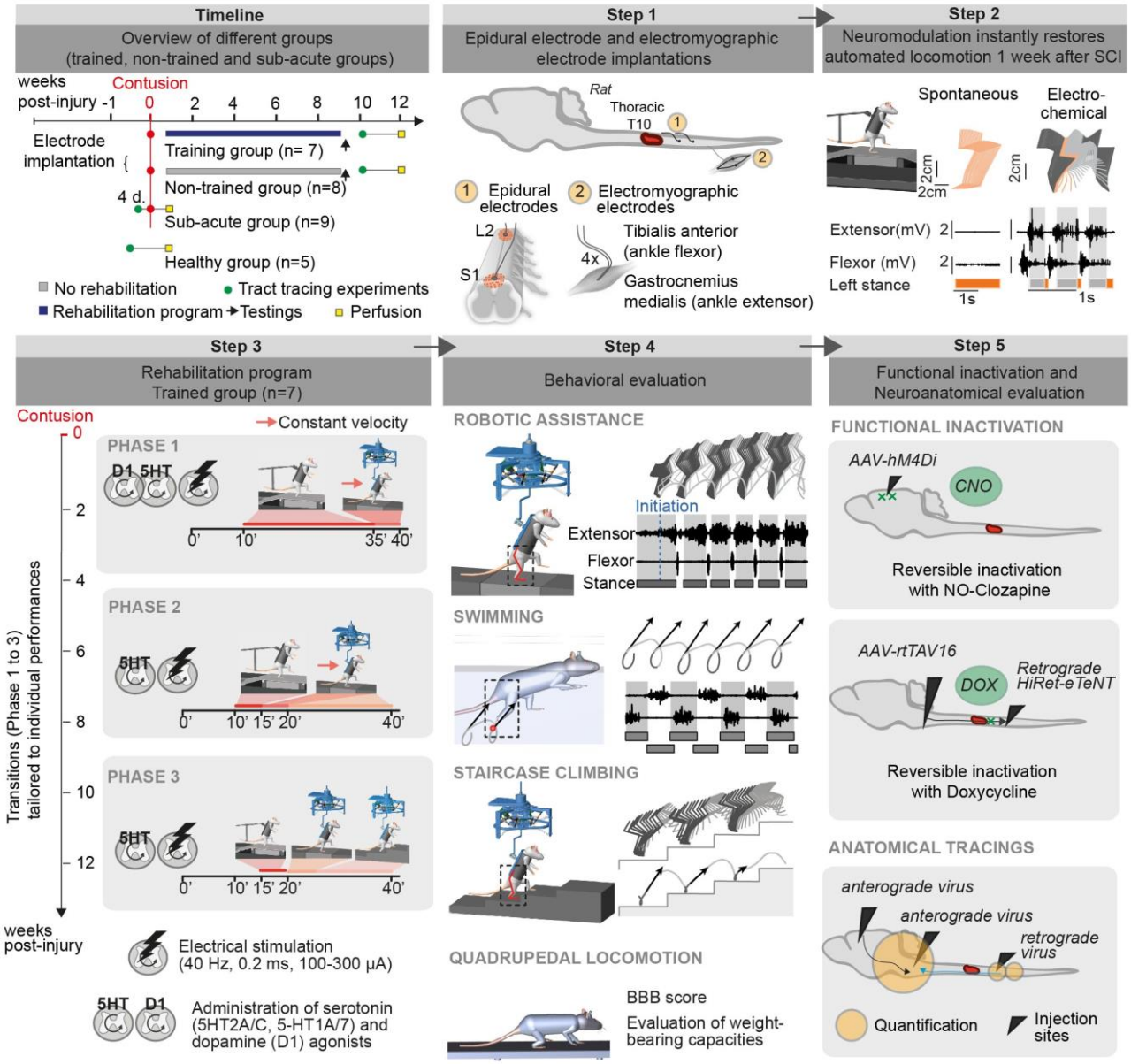

Supplementary Figure 1

General methods and experimental groups.

(**Timeline**) Summary of the experimental procedures and timeline for the main groups of animals. (**Step 1**) Surgical implantation of chronic epidural electrodes over the midline of L2 and S1 spinal cord segments to deliver electrical neuromodulation therapies. Bipolar electrodes are inserted into a pair of flexor (tibialis anterior) and extensor (medial gastrocnemius) muscles of the ankle to record electromyographic activity. (**Step 2**) A severe contusion was performed at the mid-thoracic level. Leg kinematics and muscle activity are shown for a rat tested on a treadmill 1 week after contusion, both without and with electrochemical neuromodulation. (**Step 3**) Design of the task-specific training regimen throughout the period of recovery, including the transition from automatic stepping on a treadmill to overground walking with robotic assistance, to stair climbing. The features and time-dependent adaptations of the electrochemical neuromodulation therapy are shown. Briefly, the type and concentration of administered chemicals is constantly adjusted to the current motor performance of the rats. (**Step 4**) Behavioral tasks to evaluate leg motor control. (**Step 5**) Schematic overview of the functional inactivation and anatomical experiments that were used to evaluate the reorganization of neuronal pathways.

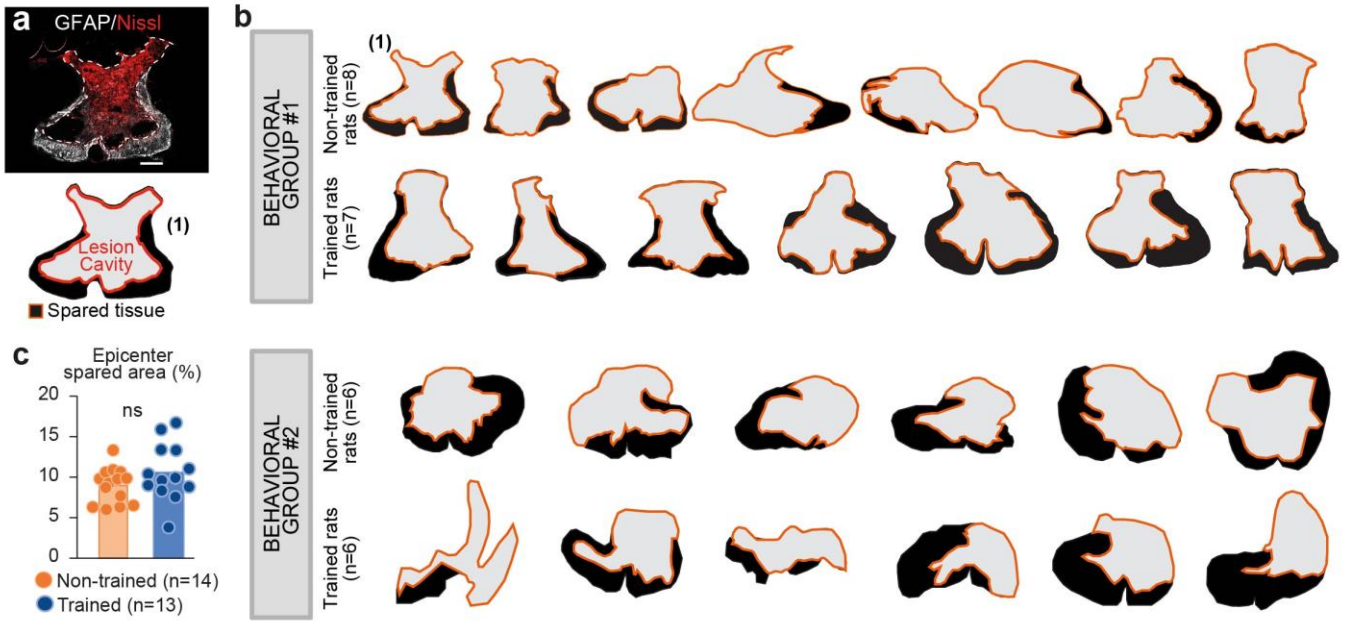

Supplementary Figure 2

Characterization of spinal cord contusion in rats.

(a) Photograph of a coronal section through the contusion epicenter (GFAP, Glial fibrillary acidic protein), which was used to trace the contour of the contusion cavity, as illustrated below. Scale bar, 250μm. **(b)** The contours of the lesion cavity at the epicenter are shown for all the main experimental rats used for behavioral and anatomical evaluations. **(c)** The bar graph reports the area of spared tissue at the lesion epicenter for pooled non-trained (n=14) and trained (n=13) rats. ns, not significant; Non-paired Student's t-test.

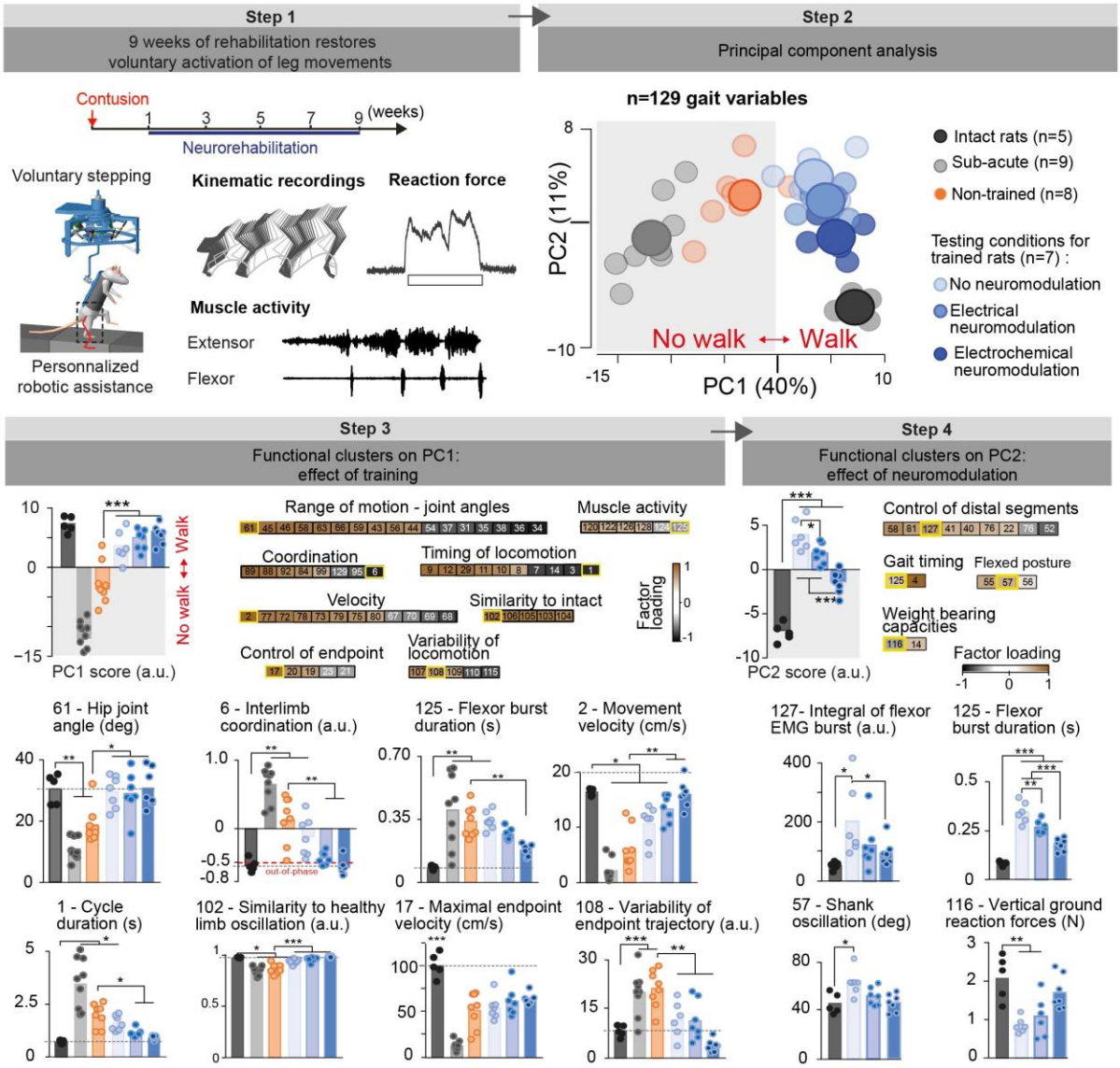

Supplementary Figure 3

Behavioral evaluations of gross and detailed motor performance.

(**Step 1**) Rats were evaluated during overground locomotion in a bipedal posture with robotic assistance. They were tested without neuromodulation, with electrical neuromodulation, and with electrochemical neuromodulation. Rats were trained to step overground with the gravity-assist during 9 weeks. Stepping performance (kinematics, muscle activity and ground reaction forces) was evaluated for different testing conditions at the end of the training period and compared to the motor output of non-trained rats. (**Step 2**) A PC analysis was applied on a total of 129 parameters characterizing global and fine details of leg motor control (**Supplementary Table 2**) **table S1**). The gait cycles of each rat under each neuromodulation condition (single dot, averaged of 10 to 20 gait cycles per rat) and averaged per group and conditions (large dots) are represented in new space defined by PC1 and PC2 (%, percent of explained variance). PC1 differentiated the effects of training, distinguishing the ability to move forward (walking) versus movements in place or falling backward (not able to walk). PC2 distinguished the effects of the neuromodulation conditions on leg motor control. (**Step 3**) The score of each rat on PC1 was extracted to quantify motor performance, i.e. the relative difference to intact (no injury) rats. The parameters that correlated highly with PC1 were extracted and regrouped in functional clusters that we named for clarity (# refers to **Supplementary Table 2**). The bar plots report the mean values for one parameter per each cluster, highlighted in yellow in the cluster. (**Step 4**) The same procedure was applied for parameters correlating with PC2, to identify the specific effects of neuromodulation conditions. *P < 0.05; **P < 0.01; ***P < 0.001. One-way ANOVA followed by Bonferroni's post-hoc test.

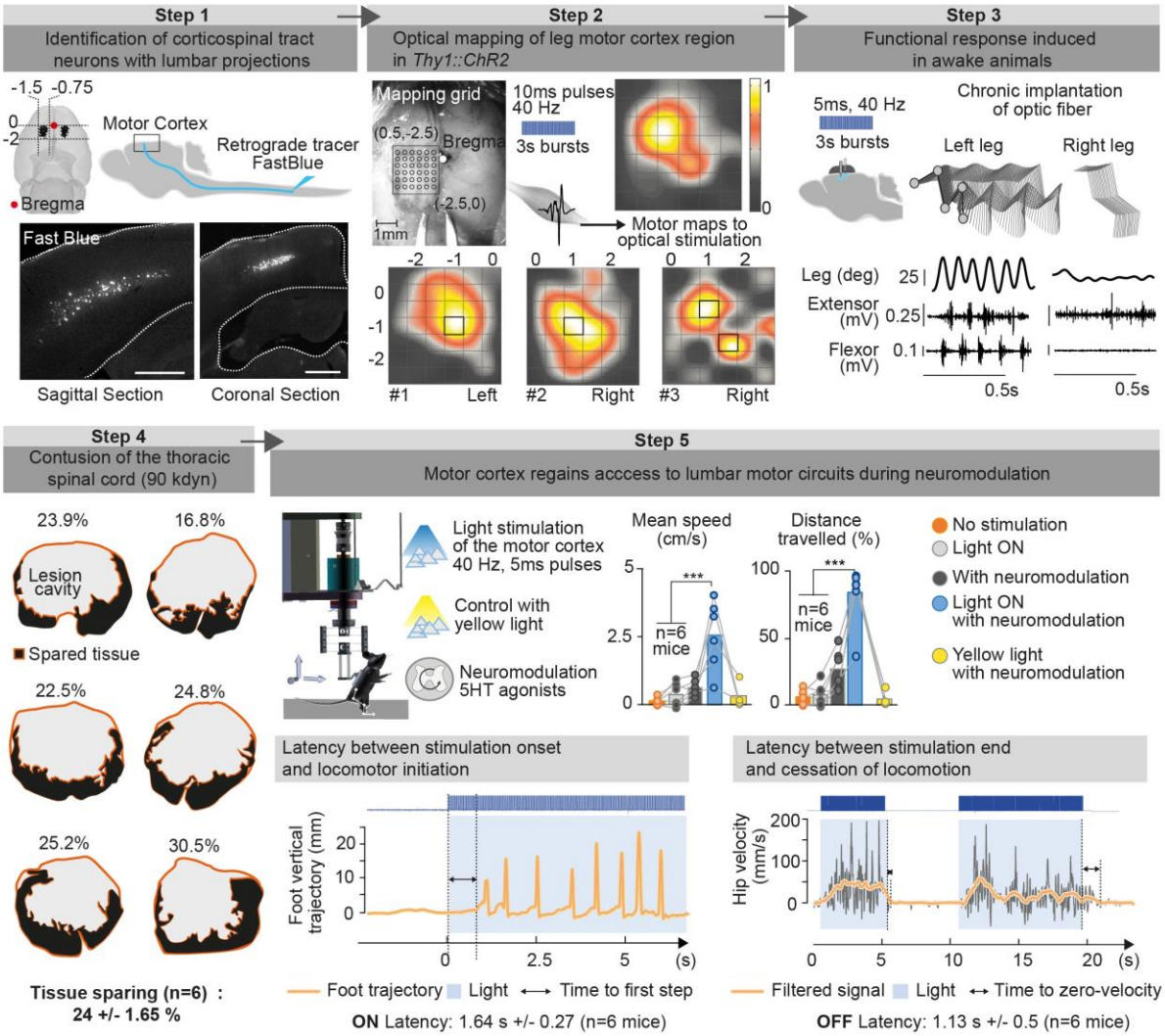

Supplementary Figure 4

Optical manipulation of leg motor cortex activity in mice.

(**Step 1**) To identify corticospinal tract neurons projecting to lumbar spinal segment, the retrograde tracer FastBlue was injected in the lumbar segments of *Thy1:ChR2-YFP* mice. Photographs show a sagittal and coronal view of FastBlue-labelled cells in the motor cortex. Scale bar 500μm. The scheme shows a 3D reconstruction of all the labelled cells. (**Step 2**) Short bursts of optical stimulation were delivered using a mapping grid positioned over the motor cortex region identified in Step1, as shown in the photograph. The amplitude of the motor evoked potentials recorded in the contralateral flexor muscles of the ankle was measured for each site of stimulation in order to elaborate a motor map for each tested mouse (bottom, squares indicate hotspots), and all mice combined (top). (**Step 3**) Optic fibers were implanted chronically in the region identified in step 2. Stick diagram decomposition of leg movements, amplitude of leg oscillations, and electromyographic activity of the tibialis anterior (flexor) and gastrocnemius medialis (extensor) of the left and right legs in response to optical stimulation of the right motor cortex in suspended, awake mice. (**Step 4**) Mice received a contusion of the spinal cord at the T9 spinal segment level. For each experimental mouse, the lesion was reconstructed in order to visualize spared tissue (black) and lesion cavity (grey). (**Step 5)** Scheme showing the experimental conditions to test the mice with contusion. Bar plots reporting the mean speed and relative travelled distance under the different experimental conditions (n=6 mice). Note the absence of behavioral effects when a non-specific yellow light was delivered over the motor cortex. ***P < 0.001. One-way ANOVA followed by Bonferroni's post-hoc test. **Bottom left,** the latency between the delivery of optical stimulation and the onset of locomotion was measured as the duration between the onset of the optical stimulation and the first vertical elevation of the foot. Bottom right, the latency between the termination of optical stimulation and the cessation of locomotion was measured as the duration between the end of the optical stimulation and the zero crossing of the filtered hip velocity profile.

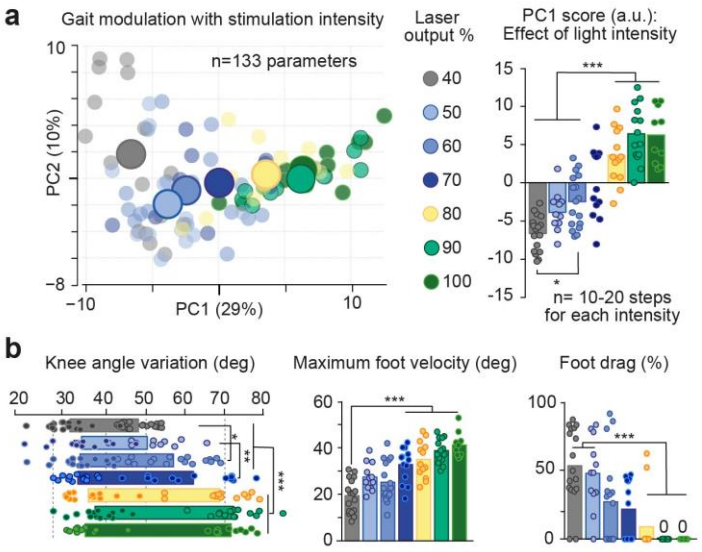

Supplementary Figure 5

The motor cortex regains adaptive control of leg movements during neuromodulation.

Leg kinematics were recorded during continuous stepping on a treadmill with different levels of optical intensities (laser output, %). A total of 133 parameters characterizing gait patterns were measured and submitted to a principal component (PC) analysis. The plot shows each gait cycle (small dot) in the new, reduced space created by PC1 and PC2. Large spots represent average per stimulation intensity. The bar plot on the right reports mean PC1 values, averaged over individual values for each gait cycle (individual dots). The number of gait cycles varies for each light intensity: n=17 steps (40%), n=11 (50%), n=17 (60%), n=13 (70%), n=13 (80%), n=14 (90%), n=10 (100%). Laser output is expressed in percentage of the maximal light intensity (60mW). **(b)** The bar plots show average values of single gait parameters for each stimulation intensity. *P < 0.05; **P < 0.01; ***P < 0.001. One-way ANOVA followed by Bonferroni's post-hoc test.

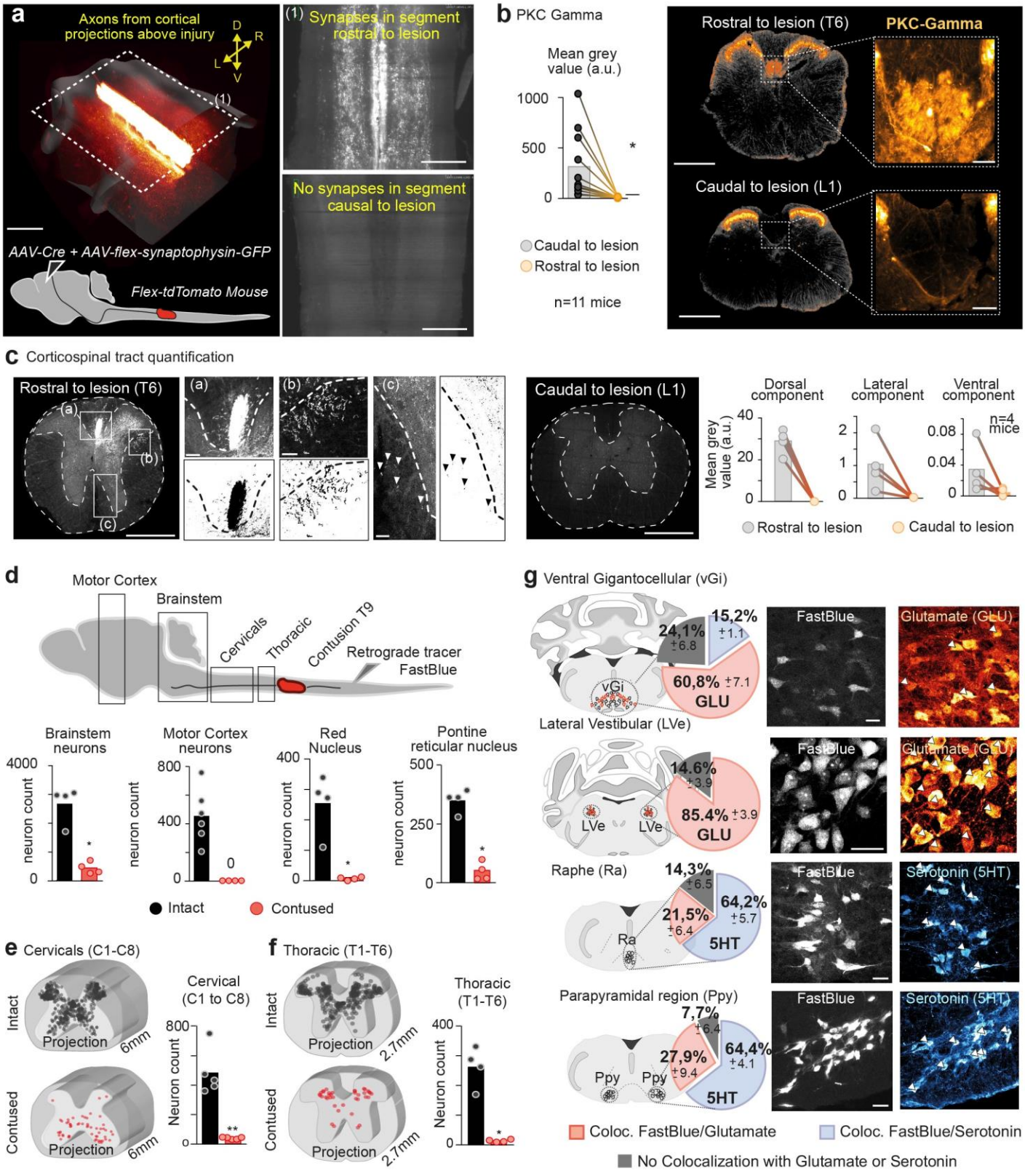
a
Axons from cortical projections above injury
D
R
L
V
(1)
AAV-Cre + AAV-flex-synaptophysin-GFP
Flex-tdTomato Mouse
(1) Synapses in segment rostral to lesion
No synapses in segment causal to lesion
b PKC Gamma
Mean grey value (a.u.)
1000
500
0
*
Caudal to lesion
Rostral to lesion
n=11 mice
Rostral to lesion (T6)
PKC-Gamma
Caudal to lesion (L1)
c Corticospinal tract quantification
Rostral to lesion (T6)
(a)
(b)
(c)
Caudal to lesion (L1)
Dorsal component
Lateral component
Ventral component
Mean grey value (a.u.)
40
20
0
2
1
0
0.08
0.04
0
n=4 mice
Rostral to lesion
Caudal to lesion
d
Motor Cortex
Brainstem
Cervicals
Thoracic
Contusion T9
Retrograde tracer FastBlue
Brainstem neurons
Motor Cortex neurons
Red Nucleus
Pontine reticular nucleus
neuron count
4000
800
400
250
500
0
*
Intact
Contused
e Cervicals (C1-C8)
Intact
Contused
Projection
6mm
Cervical (C1 to C8)
Neuron count
800
0
**
f Thoracic (T1-T6)
Intact
Contused
Projection
2.7mm
Thoracic (T1-T6)
Neuron count
400
0
*
g Ventral Gigantocellular (vGi)
24,1% ±6.8
15,2% ±1.1
60,8% ±7.1
GLU
vGi
FastBlue
Glutamate (GLU)
Lateral Vestibular (LVe)
14.6% ±3.9
85.4% ±3.9
GLU
LVe
LVe
FastBlue
Glutamate (GLU)
Raphe (Ra)
14,3% ±6.5
21,5% ±6.4
64,2% ±5.7
5HT
Ra
FastBlue
Serotonin (5HT)
Parapyramidal region (Ppy)
7,7% ±6.4
27,9% ±9.4
64,4% ±4.1
5HT
Ppy
Ppy
FastBlue
Serotonin (5HT)
Coloc. FastBlue/Glutamate
Coloc. FastBlue/Serotonin
No Colocalization with Glutamate or Serotonin

Supplementary Figure 6

Characterization of projection neurons with residual connection below the contusion in mice.

To visualize the interruption of the corticospinal tract in 3D, an AAV-Cre was co-injected with an AAV-flex-Synaptophysin-GFP into the motor cortex of *Flex-tdTomato mice* to label corticospinal tract fibers in the spinal cord. A large block of spinal cord containing the contusion was cleared using CLARITY. A representative 3D rendering of a CLARITY-processed spinal segment rostral to the contusion shows corticospinal tract fibers. Longitudinal photographs of spinal segments rostral and caudal to contusion show the synapses from corticospinal tract neurons. Scale bar 500μm. **(b)** To verify the interruption of corticospinal tract projections independent of viral injections, spinal cord sections rostral (T6) and caudal (L1) to the contusion were stained with Protein Kinase C gamma (PKC-Gamma) antibodies, which label corticospinal tract axons. The bar plot reports the mean relative (arbitrary unit, a.u.) intensity of the PKC-Gamma signal in segments caudal and rostral to the contusion. Scale bars 500μm, 50 μm insets. *P < 0.05. Paired Student's t-test. **(c)** To quantify the interruption of corticospinal tract projections from the leg region of the motor cortex, fluorescence of the main corticospinal tract component in the dorsal column, the lateral component and the ventral component was measured in spinal cord sections rostral (T6) and caudal (L1) to the contusion. Scale bars 500μm, 50 μm insets. Bar plots show the mean relative (arbitrary unit, a.u.) intensity of corticospinal tract axons projecting in the different regions of the white matter. **(d)** Diagram illustrating the injections of the retrograde tracer FastBlue in the lumbar spinal cord to identify projection neurons with residual connections below the contusion. The diagram illustrates the various regions where neurons were found and analysed. Bar plots report the number of neurons in these regions (n = 4 each for intact and contused mice). 3D cervical **(e)** and **(f)** thoracic spinal cord reconstructions in intact and contused mice, including quantifications. *P < 0.05; **P < 0.01. Mann-Whitney test. **(g)** The phenotype of brainstem neurons with residual projections below the contusion was studied with immunohistochemistry. Photographs show neurons retrogradely labelled from lumbar segments and the co-localisation with glutamate or serotonin (white arrows). Scale bars 25μm. The polar plots display the mean percentage (+- s.e.m) of neurons co-localising with glutamate or serotonin with respect to the entire population of neurons retrogradely labelled from lumbar segments in intact mice (n=4 mice).

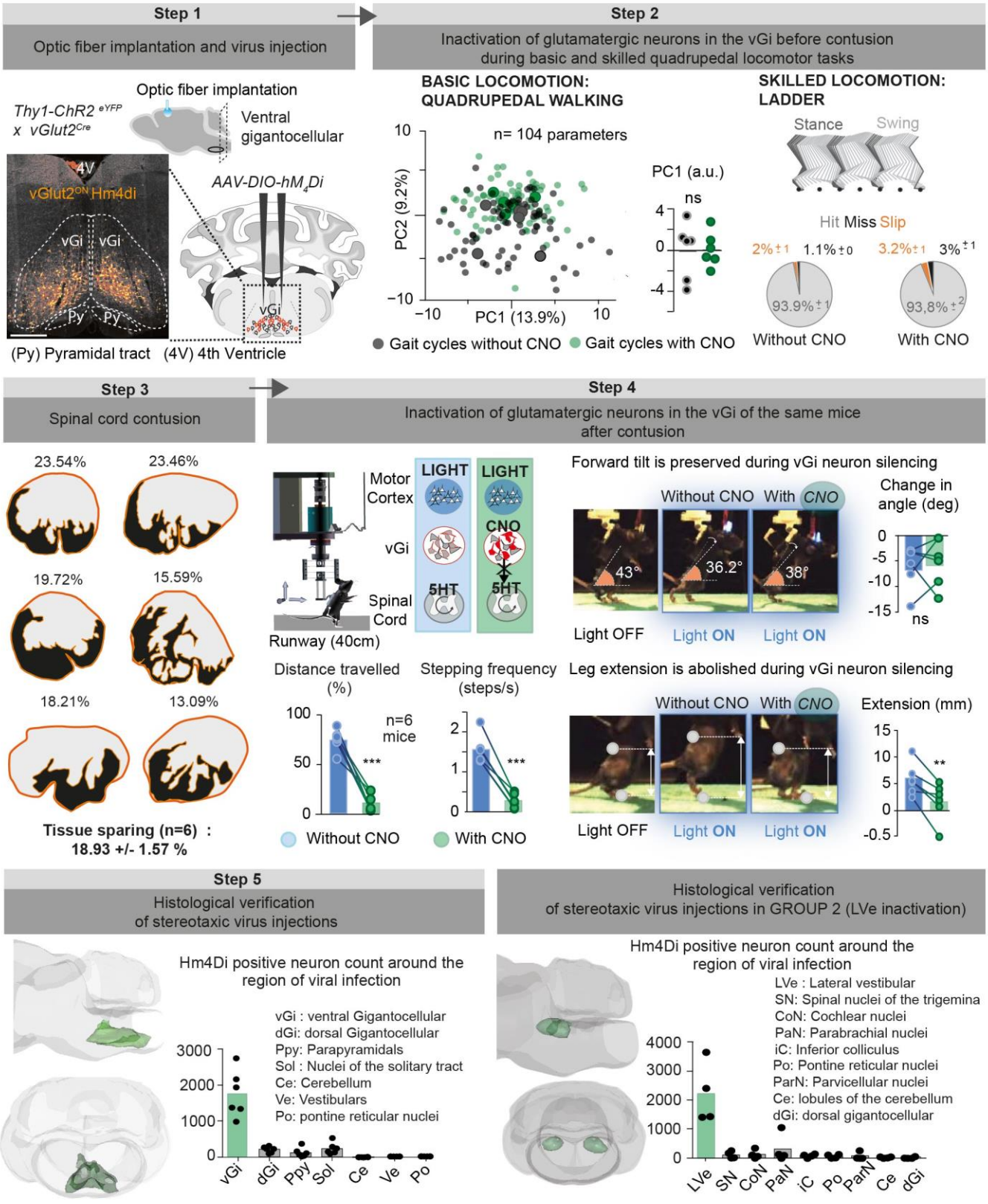
Step 1
Optic fiber implantation and virus injection
Step 2
Inactivation of glutamatergic neurons in the vGi before contusion during basic and skilled quadrupedal locomotor tasks
Optic fiber implantation
Thy1-ChR2 eYFP x vGlut2Cre
Ventral gigantocellular
4V
vGlut2ON Hm4di
vGi
vGi
Py
Py
AAV-DIO-hM4Di
vGi
(Py) Pyramidal tract
(4V) 4th Ventricle
BASIC LOCOMOTION: QUADRUPEDAL WALKING
n= 104 parameters
PC2 (9.2%)
PC1 (13.9%)
PC1 (a.u.)
ns
Gait cycles without CNO
Gait cycles with CNO
SKILLED LOCOMOTION: LADDER
Stance
Swing
Hit Miss Slip
2%±1
1.1%±0
3.2%±1
3%±1
93.9%±1
93,8%±2
Without CNO
With CNO
Step 3
Spinal cord contusion
Step 4
Inactivation of glutamatergic neurons in the vGi of the same mice after contusion
23.54%
23.46%
19.72%
15.59%
18.21%
13.09%
Tissue sparing (n=6) :
18.93 +/- 1.57 %
Motor Cortex
vGi
Spinal Cord
Runway (40cm)
LIGHT
LIGHT
CNO
5HT
5HT
Forward tilt is preserved during vGi neuron silencing
Without CNO
With CNO
43°
36.2°
38°
Light OFF
Light ON
Light ON
Change in angle (deg)
ns
Distance travelled (%)
n=6 mice
***
Stepping frequency (steps/s)
***
Without CNO
With CNO
Leg extension is abolished during vGi neuron silencing
Without CNO
With CNO
Light OFF
Light ON
Light ON
Extension (mm)
**
Step 5
Histological verification of stereotaxic virus injections
Hm4Di positive neuron count around the region of viral infection
vGi : ventral Gigantocellular
dGi: dorsal Gigantocellular
Ppy: Parapyramidals
Sol : Nuclei of the solitary tract
Ce: Cerebellum
Ve: Vestibulars
Po: pontine reticular nuclei
vGi
dGi
Ppy
Sol
Ce
Ve
Po
Histological verification of stereotaxic virus injections in GROUP 2 (LVe inactivation)
Hm4Di positive neuron count around the region of viral infection
LVe : Lateral vestibular
SN: Spinal nuclei of the trigemina
CoN: Cochlear nuclei
PaN: Parabrachial nuclei
iC: Inferior colliculus
Po: Pontine reticular nuclei
ParN: Parvicellular nuclei
Ce: lobules of the cerebellum
dGi: dorsal gigantocellular
LVe
SN
CoN
PaN
iC
Po
ParN
Ce
dGi

Supplementary Figure 7

Inactivation of vGi neurons suppresses cortical control of locomotion.

(**Step1**) Strategy to express DREADDs specifically in glutamatergic neurons of the vGi, while manipulating the activity of motor cortex projection neurons with light (n = 6 mice). Photograph showing expression of *hM4Di* in *vGluT2^{ON}* vGi neurons. Scale bar, 500μm. (**Step 2**) Intact (no injury) mice were tested before and after CNO during quadrupedal locomotion along a flat surface and a horizontal ladder. A PC analysis was applied on 104 gait parameters (see **Supplementary Table 2**) characterizing the walking pattern. Gait cycles (small dot, individual gait cycles; large dots, average per mouse and condition) measured along the flat surface are represented in the new space created by PC1 and PC2 (%, explained variance). No significant difference was detected between both conditions. The stick diagram decomposition of leg movements shows the progression along the horizontal ladder. The polar plot reports the mean relative percent of hits, misses and slips onto the rungs of the ladder for both conditions (+- s.e.m). Silencing *vGluT2^{ON}* vGi neurons did not alter skilled leg movements. (**Step 3**) The same mice received a severe contusion. For each experimental mouse, the lesion was reconstructed in order to visualize spared tissue (black) and lesion cavity (grey). (**Step 4**) Experimental conditions to evaluate the cortical control of leg movements before and after silencing *vGluT2^{ON}* vGi neurons. Mice were tested bipedally under chemical neuromodulation (5HT agonists). The bar plots represents the mean distance travelled and the mean stepping frequency when delivering optical motor cortex stimulation without and with CNO (n=6 mice). The snapshots illustrate the forward tilt of the trunk and whole leg extension when delivering optical stimulation. The bar plots report the mean values of these parameters (n=6 mice). **P < 0.01; ***P < 0.001. Two-tailed paired Student's t-test. (**Step 5**) Post-mortem evaluation of hM4Di positive neurons in the vGi and potential infection in neighbouring regions for all experimental animals (n=6 mice), shown as mean +- s.e.m. The coronal and dorsoventral snapshots of the brainstem show the 3D volume containing *vGluT2^{ON} hM4Di* expressing neurons. Post-mortem evaluation of hM4Di positive neurons in the lateral vestibular nuclei (n=4 mice) shown as mean +- s.e.m., and 3D volume containing *vGluT2^{ON} hM4Di* expressing neurons is shown in the right panel.

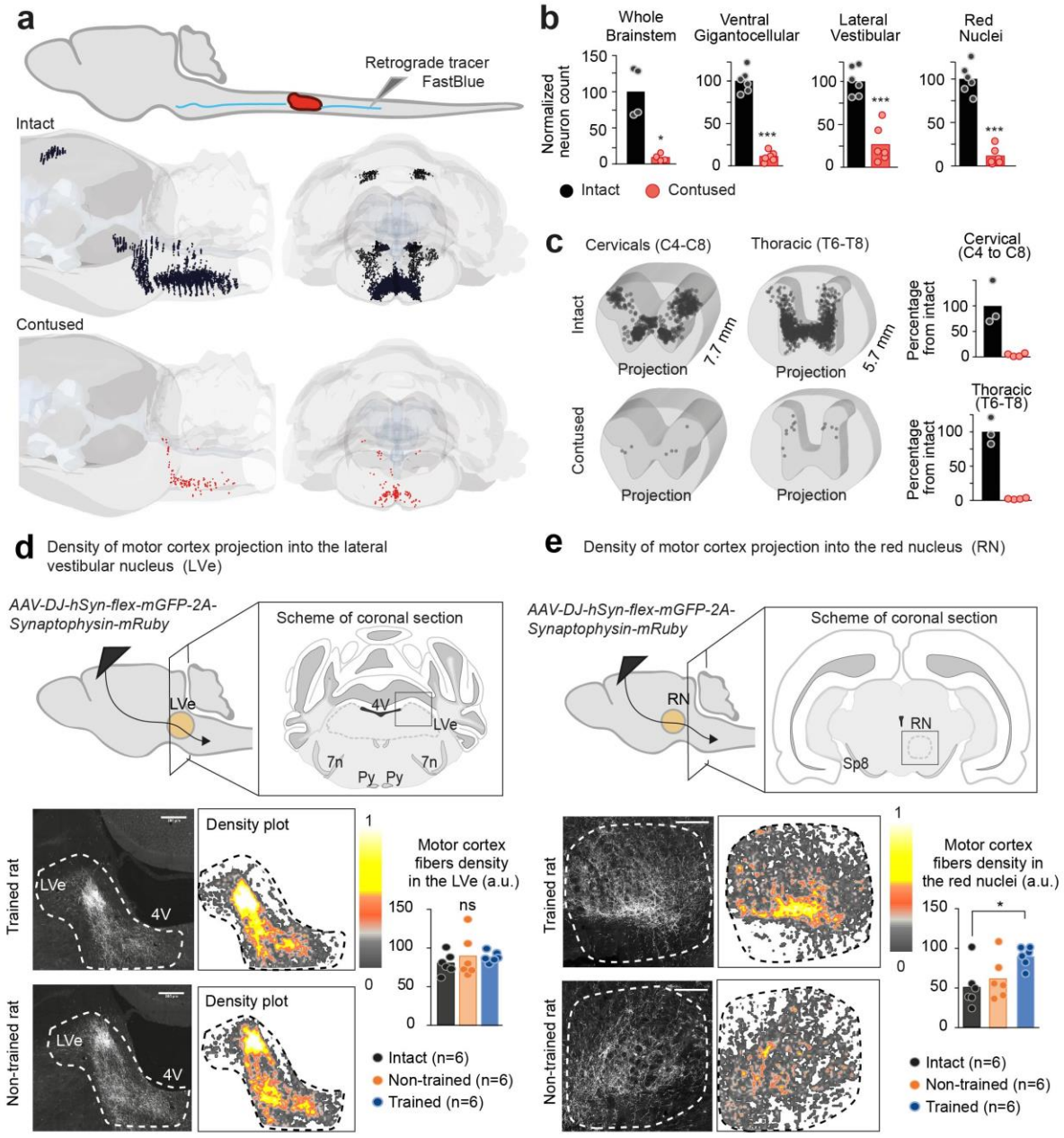

Supplementary Figure 8

Characterization of projection neurons with residual connection below the contusion in rats, and reorganization of motor cortex projections in the brainstem.

(**a**) Diagram illustrating the injections of the retrograde tracer FastBlue in the lumbar spinal cord to identify projection neurons with residual connections below the contusion in rats. Coronal and dorsoventral snapshots of 3D brain and brainstem reconstructions in intact and contused (non-trained) rats. Each neuron is represented by a single dot. **(b)** The bar plots report the relative number of identified neurons in the whole brainstem (n = 4 each for intact and contused rats) and selected regions from the brainstem (n=6 each for intact and contused). **(c)** 3D cervical and thoracic spinal cord reconstructions in intact and contused rats, including quantifications. *P < 0.05;**P < 0.01; ***P < 0.001. Non-paired Student's t-test (b) or Mann-Whitney test (c). **(d and e)** Scheme illustrating motor cortex injections and regions for the quantification of motor cortex projections. Representative photographs and corresponding heat maps of motor cortex projections in the lateral vestibular nuclei **(d)** and red nuclei **(e)** of intact (n=6), non-trained (n=6) and trained (n=6) rats. Scale bars, 200μm. *P < 0.05, One-way ANOVA followed by Bonferroni's post-hoc test.

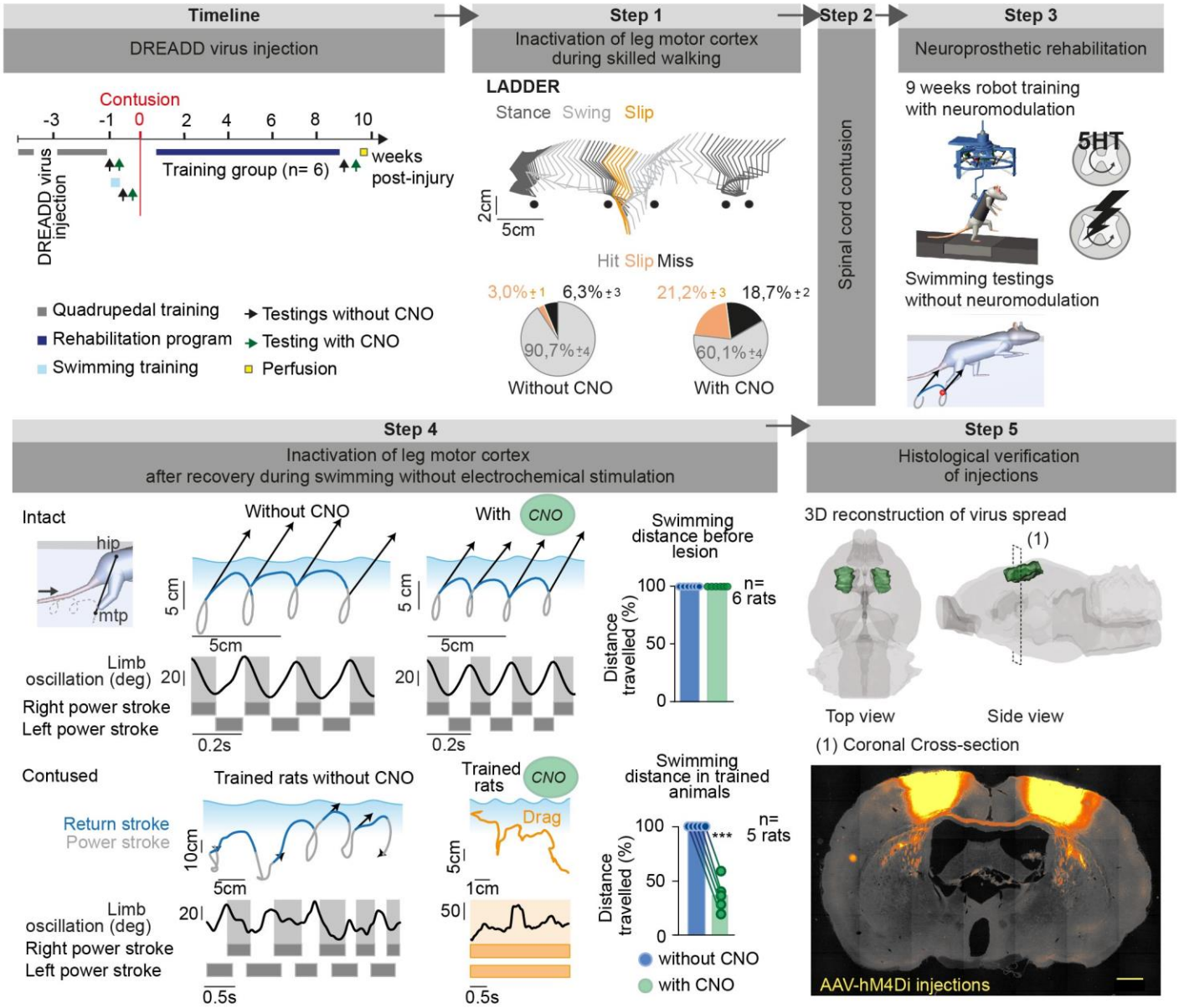
Timeline
DREADD virus injection
Contusion
-3 -1 0 2 4 6 8 10
weeks post-injury
DREADD virus injection
Training group (n= 6)
Quadrupedal training
Rehabilitation program
Swimming training
Testings without CNO
Testing with CNO
Perfusion
Step 1
Inactivation of leg motor cortex during skilled walking
LADDER
Stance Swing Slip
2cm
5cm
Hit Slip Miss
3,0%±1 6,3%±3
90,7%±4
Without CNO
21,2%±3 18,7%±2
60,1%±4
With CNO
Step 2
Spinal cord contusion
Step 3
Neuroprosthetic rehabilitation
9 weeks robot training with neuromodulation
5HT
Swimming testings without neuromodulation
Step 4
Inactivation of leg motor cortex after recovery during swimming without electrochemical stimulation
Intact
hip
mtp
Without CNO
With CNO
5 cm
5cm
Limb oscillation (deg)
20
Right power stroke
Left power stroke
0.2s
Contused
Trained rats without CNO
Trained rats
CNO
Drag
Return stroke
Power stroke
10cm
1cm
50
0.5s
Swimming distance before lesion
Distance travelled (%)
100
50
0
n= 6 rats
Swimming distance in trained animals
***
n= 5 rats
without CNO
with CNO
Step 5
Histological verification of injections
3D reconstruction of virus spread
(1)
Top view
Side view
(1) Coronal Cross-section
AAV-hM4Di injections

Supplementary Figure 9

Silencing of leg motor cortex neurons abolishes leg motor control in trained rats.

(**Timeline**) Timeline of experimental procedures in intact (n = 6) and contused rats (n = 5). (**Step 1**) Intact rats were evaluated during locomotion along the irregularly spaced rungs of a ladder, before and after CNO administration. The circular plots report the percent of hits, misses and slips onto the rungs of the ladder for both conditions. (**Step 2**) The rats received a 250 kdyn contusion. (**Step 3**) They followed the standard neurorehabilitation protocols as described in **Supplementary Fig. 2**. (**Step 4**) Stick diagram decomposition of leg movements during swimming. Successive leg endpoint trajectories, including velocity vector at return stroke onset, together with the oscillation of the limb and occurrence of left and right power strokes during swimming. A representative sequence is shown for intact and contused rats, both without and with CNO. Contused rats were tested without neuromodulation. ***P < 0.001. Paired Student's *t*-test. (**Step 5**) 3D reconstruction of the cortical region with neurons expressing *hM4Di*, including a photograph through the coronal plane marked (1). Scale bar, 500μm.

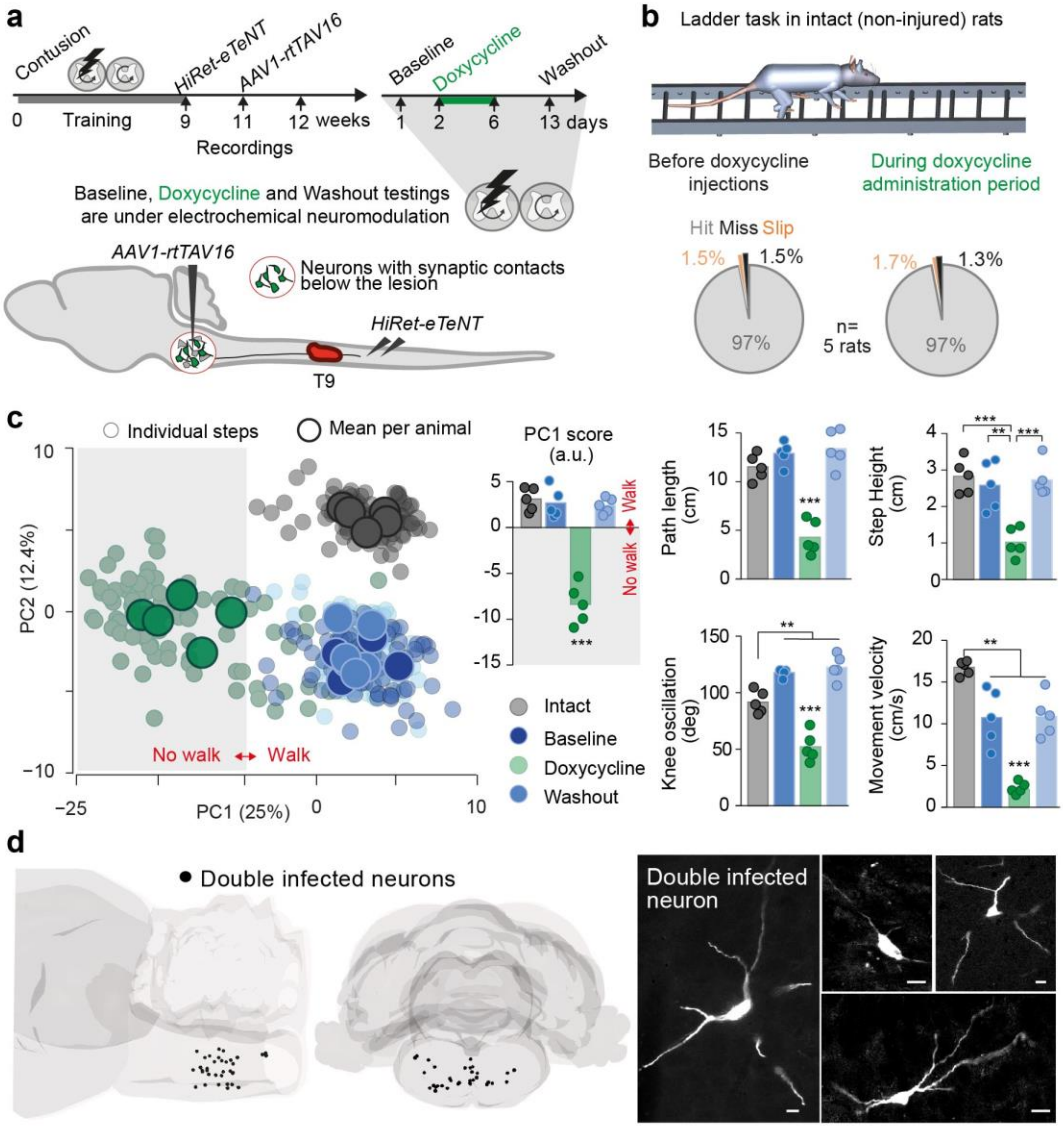

Supplementary Figure 10

Inactivation of vGi neurons projecting below the contusion abolishes leg motor control in trained rats.

(**a**) Timeline of experimental procedures and strategy for the reversible inactivation of vGi neurons with projections to lumbar segments, both in intact (n = 5 rats) and contused rats (n = 5 rats). (**b**) Intact rats (no injury) were evaluated during locomotion along the irregularly spaced rungs of a ladder, before and after repeated doxycycline administration. The circular plots report the percent of hits, misses and slips onto the rungs of the ladder for both conditions (**c**) PC analysis using the same conventions as in **Fig. 1**. All the individual gait cycles are shown, as well as the average for each rat. The bar plot near the PC analysis reports the mean values of the score on PC1, which differentiated trials with forward progression (walking) from trials without initiation (not walking). The other bar plots report the mean values of basic gait parameters illustrating the robust deterioration of leg motor control during inactivation of vGi neurons with residual projections to lumbar segments in trained rats. **P < 0.01; ***P < 0.001. One-way ANOVA followed by Bonferroni's post-hoc test.(**d**) 3D reconstruction of all neurons expressing both transgenes, including photographs showing the morphology of these neurons. Scale bars, 25μm.

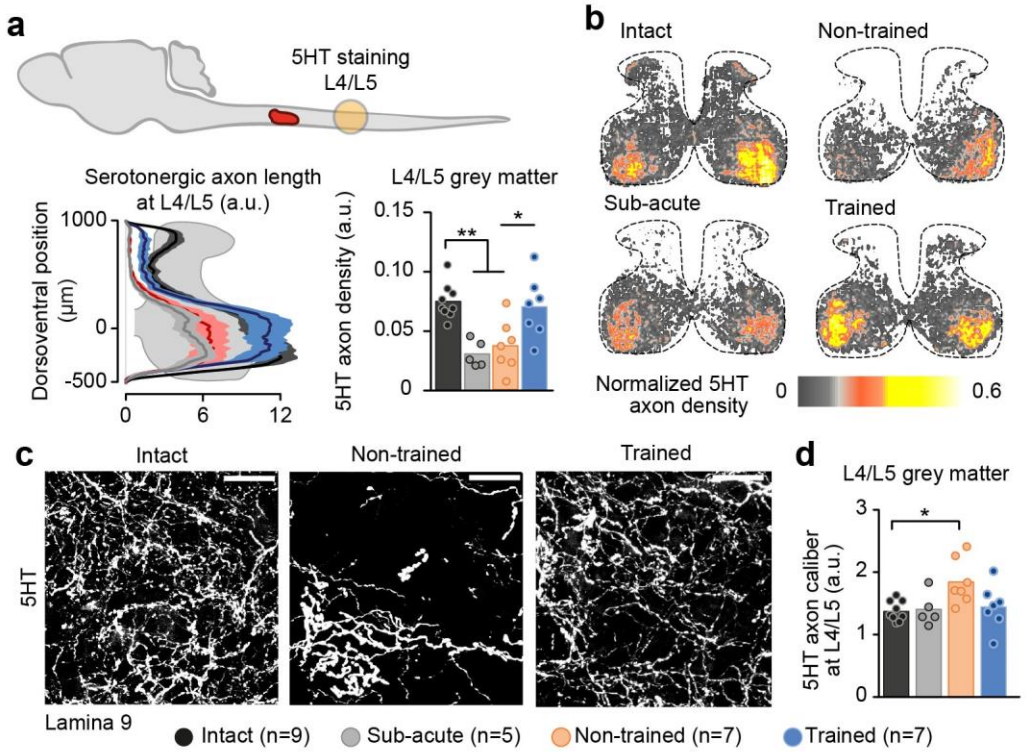

Supplementary Figure 11

Reorganization of serotonergic (5HT) axons in the lumbar spinal cord.

(a) Scheme showing the location at which the density of 5HT axons was evaluated. Density plot of 5HT axons along the dorsoventral extent of the spinal cord (bold line represents the mean distribution for all animals, shaded region represents s.e.m.), and bar graphs reporting the mean axon density of 5HT axons and individual animals within L4/L5 spinal segments. **(b)** Representative heat maps of 5HT axons, visualized at L4/L5. **(c)** Representative images of 5HT axons in the lamina 9 of L4 segment. Scale bar, 25 µm (d) Bar graph reporting the mean caliber of 5-HT axons at L4/L5. Scale bars, 25µm.*P < 0.05; **P < 0.01. One-way ANOVA followed by Bonferroni's post-hoc test.

Supplementary Table 1: Overview of experimental groups.

OVERVIEW OF GROUPS					
SPECIES	**ANALYSIS**	**GROUP**	**N**	**FIGURE NUMBER**	**EPICENTER SPARED AREA (mean +- s.e.m.)**
RATS	Behavioral assessments and quantification of vGi projections in the spinal cord	INTACT SUB-ACUTE NON-TRAINED TRAINED	5 9 8 7	Fig.1, Fig. 2b-2f, Fig. 8a Sup. Fig.1, Sup. Fig. 3	- 12.7 +- 1.1 8.04 +- 0.7 12.29 +- 1.2
	Supplementary behavioral assessments and quantification of cortical projections in the brainstem	INTACT NON-TRAINED TRAINED	6 6 6	Fig.2d, Fig. 7a Sup. Fig. 8	- 10.26 +- 0.61 8.66 +- 1.16
	Hindlimb motor cortex inactivation with DREADDs	TRAINED	5	Fig.7b Sup. Fig. 9	9.93 +- 0.89
	Inactivation of vGi neurons with synaptic inputs to the lumbar spinal cord	TRAINED	5	Fig.8c Sup. Fig. 10	N/A
MICE	Motor cortex activation after contusion	CONTUSED	6	Fig. 3c-3d Sup. Fig. 4, Sup. Fig. 5	23.97 +- 1.65
	Inactivation of glutamatergic neurons in the vGi with DREADDs	CONTUSED	6	Fig. 5b-5c Sup. Fig. 7	18.93 +- 1.57
	Inactivation of glutamatergic neurons in the LVe with DREADDs	CONTUSED	4	Fig. 5d Sup. Fig. 7	20.83 +- 2.50

Supplementary Table 2: Kinematic, Kinetic and EMG parameters.

#		Computed parameter
Rat	Mouse	Gait Timing
1	1	Cycle duration
2	2	Movement velocity
3	3	Stance duration
4	4	Swing duration
5	5	Stance duration in percentage of whole cycle
6	6	Interlimb coordination
7	7	Double stance (in percentage of gait cycle duration)
8	8	Stride length
9	9	Step length
10	10	Step height
11	11	Step height normalized to stance height
12	12	Path length
		Endpoint trajectory shape
13	13	Stance width
14		Body weight support by the postural prosthesis
15	14	Maximal backward position of the foot
16	15	Maximal forward position of the foot
17	16	Maximal endpoint velocity
18	17	Timing of the maximal enpoint velocity
19	18	Endpoint acceleration
20	19	Endpoint velocity
21	20	orientation of the velocity vector at swing onset
22		Drag duration
23		relative drag dura on (percent of swing duration)
		Stability
24	21	Amplitude of lateral trunk position
25	22	Sagital trunk movement
26	23	Sagital trunk velocity
27	24	Variability of vertical hip-midpoint oscillation
28	25	Variability of medio-lateral hip rotation
29	26	Forward movement of the center of mass
30	27	Lateral oscillation of the center of mass
		Joint angles and limb segment oscillations
31	28	Crest oscillation (minimal elevation)
32	29	thigh oscillation (minimal elevation)
33	30	Shank oscillation (minimal elevation)
34	31	Foot oscillation (minimal elevation)
35		Toe oscillation (minimal elevation)
36	32	Whole limb oscillation (minimal elevation)
37	33	Crest oscillation (maximal elevation)
38	34	thigh oscillation (maximal elevation)
39	35	Shank oscillation (maximal elevation)
40	36	Foot oscillation (maximal elevation)
41		Toe oscillation (maximal elevation)
42	37	Whole limb oscillation (maximal elevation)
43	38	Hip joint angle (maximal)
44	39	Knee joint angle (maximal)
45	40	Ankle joint angle (maximal)
46		MTP joint angle (maximal)
47	41	Whole limb adduction
48	42	Foot adduction
49	43	Hip joint angle (minimal)
50	44	Knee joint angle (minimal)
51	45	Ankle joint angle (minimal)
52		MTP joint angle (minimal)
53	46	Whole limb abduction
54	47	Foot abduction
55	48	Crest oscillation
56	49	Thigh oscillation
57	50	Shank oscillation
58	51	Foot oscillation
59		Toe oscillation
60	52	Whole limb oscillation
61	53	Hip joint angle
62	54	Knee joint angle
63	55	Ankle joint angle
64	56	MTP joint angle
65	57	Whole limb medio-lateral oscillation
66	58	Foot rotation

		Velocity
67	59	Whole limb angle velocity (minimal)
68	60	Hip joint anlge velocity (minimal)
69	61	Knee joint angle velocity (minimal)
70	62	Ankle joint angle velocity (minimal)
71		MTP joint angle velocity (minimal)
72	63	Whole limb angle velocity (maximal)
73	64	Hip joint anlge velocity (maximal)
74	65	Knee joint angle velocity (maximal)
75	66	Ankle joint angle velocity (maximal)
76		MTP joint angle velocity (maximal)
77	67	Whole limb angle velocity
78	68	Hip joint anlge velocity
79	69	Knee joint angle velocity
80	70	Ankle joint angle velocity
81		MTP joint angle velocity
		(Intra-limb) coordination
82	71	Temporal coupling between crest and thigh oscillation
83	72	Temporal coupling between thight and shank oscillation
84	73	Temporal coupling between shank and foor oscialltion
85		Temporal coupling between foot and toe oscillation
86	74	correlation of crest and thigh oscillation
87	75	Correlation of thigh and leg oscillation
88	76	Correlation of leg and foot oscillation
89		Correlation of foot and toe oscillation
90	77	Correlation of hip and knee oscillation
91	78	Correlation of knee and ankle oscillation
92	79	Correlation of ankle and MTP oscillation
93	80	Timing of crest-thigh (minimal)
94	81	Timing of crest-thigh (maximal)
95	82	Timing of thigh-shank (minimal)
96	83	Timing of thigh-shank (maximal)
97	84	Timing of shank-foot (minimal)
98	85	Timing of shank-foot (maximal)
99		Degree of linear coupling between joint oscillations (PC1)
100		Degree of linear coupling between joint oscillations (PC2)
101		Degree of linear coupling between joint oscillations (PC3)
		Similarity to healthy gait
102		Correla on between limb oscillation of healthy and injured leg
103		Correla on between hip oscillation of healthy and injured leg
104		Correla on between knee oscillation of healthy and injured leg
105		Correla on between ankle oscillation of healthy and injured leg
106		Correla on between MTP oscillation of healthy and injured leg
		Variability of gait
107	86	Variability of foot trajectory in the forward direction
108	87	Variability of foot trajectory in the sagital place
109	88	Variability of foot trajectory in the 3-dimensioal room
110	89	Variability of gait cycle duration
111	90	Variability of stride length
112	91	Variability of double stance duration
113	92	Variability of step height
114	93	Variability of path length
115	94	Variability of max endpoint velocity
		Kinetics
116		vertical ground reaction force
		Muscle activity parameters
117		Burst onset of extensor
118		Burst end of extenson
119		Burst duration of extensor
120		Mean amplitude of extensor
121		Integral of extensor activity
122		Root mean square of extensor activity
123		Burst onset flexor
124		Burst end of flexor
125		Burst duration of flexor
126		Mean amplitude of flexor
127		Integral of flexor activity
128		Root mean square of eflexor activity
129		Co-contraction of the flexor and extensor muscle

Supplementary Table 3: Overview of statistics

Figure Panel	Sample Size	Description of sample collection	Statistical test	Multiple comparison	P-value
1e	5,9,8,7	Rats, average of 10-15 steps	One-Way ANOVA	Bonferroni	p < 0.0001
2b	7	Rats, average of 5-6 steps	two-tailed, paired t-test		p=0.0055
2f (Co-co)	3,8,7	Rats, average of 15 strokes	One-Way ANOVA	Bonferroni	p=0.0039
2f (Range of motion)	3,8,7	Rats, average of 15 strokes	One-Way ANOVA	Bonferroni	p < 0.0001
3c	6	Mice, average of 3-5 runs per mouse	Repeated measure, One way ANOVA	Bonferroni	p < 0.0001
3e (Extensor)	1	Mouse, 32 steps	p-value on linear regression		p < 0.0001
3e (step height)	4	Mice, 30-40 steps per mouse.	p-value on linear regression		p < 0.0001
4b	5	Mice, 1 slice above and below injury.	no test due to 0 value below injury		
4d	4,4	Mice, cumulation of neuron count from same number of slices per region for each animal	two-tailed, Mann-whitney test		p <0.05 for all regions
5b (distance)	6	Mice, 5 runs per animal	two-tailed paired t-test		p=0.0004
5b (ste. Freq.)	6	Mice, 5 runs per animal	two-tailed paired t-test		p=0.0002
5c (latency)	4,4	Mice, average of 10 repetitions	two-tailed, Mann-whitney test		p=0.0286
5c (RMS)		Mice, average of 10 repetitions	Kruskal-Wallis	Dunn's	p=0.0102
5d (distance)	4	Mice, 5 runs per animal	two-tailed,Wilcoxon signed-rank test		p=0.25
5d (speed)	4	Mice, 5 runs per animal	two-tailed,Wilcoxon signed-rank test		p=0.375
6f	5	Mice, 1 slice per animal	two-tailed paired t-test		p=0.0011
7a	6,6,6	Rats, 2 slices per animal	One-Way ANOVA	Bonferroni	p=0.107
7b	5	Rats, average of 4-5 runs per rat	two-tailed paired t-test		p=0.0007
8a (T12 level)	8,8,14,14	Rat hemicord cross-sections (right and left), average of 3 sections	One-Way ANOVA	Bonferroni	p=0.0032
8a (L4 level)	8,8,14,14	Rat hemicord cross-sections (Right and left), average of 3 sections	One-Way ANOVA	Bonferroni	p=0.0024
8c	5	Rats, average of 4-5 runs per condition and per rat	Repeated measure, One way ANOVA	Bonferroni	p<0.0001
Sup 2	14,13	Rats, 1 slice at epicenter per animal	two-tailed unpaired t-test		p=0.1583
Sup 3, Step 3 (all variables)	5,9,8,7	Rats, average of 10-15 steps	One-Way ANOVA	Bonferroni	p < 0.0001 for all
Sup 3, Step 4 (PC2)	5,7	Rats, average of 10-15 steps. Intact compared to trained tested in 3 different conditions	One-Way ANOVA	Bonferroni	p <0.0001
Sup3, Step 4 (all variables)	5,7	Rats, average of 10-15 steps. Intact compared to trained tested in 3 different conditions	One-Way ANOVA	Bonferroni	#127:p =0.0124 #125: p < 0.0001 #57: p=0.0039 #116: p=0.0034
Sup4, Step 5 (mean speed)	6,6,6,4	Mice, average of 4-5 runs per mouse	One-Way ANOVA	Bonferroni	p < 0.0001

Sup4, Step 5 (distance)	6,6,6,4	Mice, average of 4-5 runs per mouse	One-Way ANOVA	Bonferroni	$p < 0.0001$
Sup 5a	1	Mouse, 10-20 steps per light intensity	One-Way ANOVA	Bonferroni	$p < 0.0001$
Sup 5b	1	Mouse, 10-20 steps per light intensity	One-Way ANOVA	Bonferroni	$p < 0.0001$ for all parameters
Sup 6b (PKC Gamma)	11	Mice, 1 slice per mouse (Above and below injury)	two-tailed, paired t-test		$p=0.0124$
Sup 6c (CST qtif)	4	Mice, 1 slice per mouse (Above and below injury)	Comparison to 0 values		n/a
Sup 6d	4,4	Mice, cumulation of neuron count from same number of slices per region for each animal	two-tailed, Mann-whitney test		$p < 0.05$
SUP 6d (Motor cortex)	5,4	Mice, cumulation of neuron count from same number of slices per region for each animal	n/a because 0 neurons in contused animals		n/a
Sup 6e (cervical)	5,5	Mice, cumulation of 37 slices per mouse	two-tailed, Mann-whitney test		$p=0.0079$
Sup 6f (thoracic)	4,4	Mice, cumulation of 17 slices per mouse	two-tailed, Mann-whitney test		$p=0.0286$
Sup 7, step 2	6	Mice, average of 10 steps per mouse	two-tailed, paired t-test		$p=0.9322$
Sup 7, step 4 (distance)	6	Mice, average of 4-5 runs per mouse	two-tailed, paired t-test		$p=0.0004$
Sup 7, step 4 (step. Freq.)	6	Mice, average of 4-5 runs per mouse	two-tailed, paired t-test		$p=0.0002$
Sup 7, step 4 (angle)	6	Mice, average of 3-4 images per mouse	two-tailed, paired t-test		$p=0.7035$
Sup 7, step 4 (extension)	6	Mice, average of 3-4 images per mouse	two-tailed, paired t-test		$p=0.0078$
Sup 8b (BS)	4,4	Rats, cumulation of neuron count from same number of slices per region for each animal	two-tailed, Mann-whitney test		$p=0.0286$
Sup 8b (vGi, Lve, RN)	6,6	Rats, cumulation of neuron count from same number of slices per region for each animal	two-tailed, unpaired t-test		$p < 0.0001$ for all
Sup 8c (cervical)	3,4	Rats, cumulation of 48 slices per rat	two-tailed, Mann-whitney test		$p=0.0571$
Sup 8c (thoracic)	3,4	Rats, cumulation of 36 slices per rat	two-tailed, Mann-whitney test		$p=0.0571$
Sup 8d	6,6,6	Rats, 1 slice per animal	One-Way ANOVA	Bonferroni	$p=0.6662$
Sup 8e	6,6,6	Rats, 1 slice per animal	One-Way ANOVA	Bonferroni	$p=0.0310$
Sup 9	5	Rats, average of 4-5 runs per rat	two-tailed, paired t-test		$p=0.0007$
Sup 10 (PC1)	5,5,5,5	Rats, average of 15 steps per rat	One-Way ANOVA	Bonferroni	$p< 0.0001$
Sup 10 (all parameters)	5,5,5,5	Rats, average of 15 steps per rat	One-Way ANOVA	Bonferroni	Path length: $p<0.0001$ Step height: $p=0.0001$ Limb amp: $p=0.0002$ velocity: $p<0.0001$
Sup 11 (axon density)	9,5,7,7	Rats, average of 3 slices per animal	One-Way ANOVA	Bonferroni	$p=0.0003$
Sup 11 (axon caliber)	9,5,7,7	Rats, average of 3 slices per animal	One-Way ANOVA	Bonferroni	$p=0.0191$